Electrokinetics of Diffuse Soft Interfaces. 2. Analysis Based on the Nonlinear Poisson−Boltzmann Equation

1 AUTHOR:

Jerome F.L. Duval
French National Centre for Scientific Research
111 PUBLICATIONS **1,941** CITATIONS

SEE PROFILE

Electrokinetics of Diffuse Soft Interfaces. 2. Analysis Based on the Nonlinear Poisson−Boltzmann Equation

Jérôme F. L. Duval*

Department of Physical Chemistry and Colloid Science, Wageningen University, Dreijenplein 6, 6703 HB Wageningen, The Netherlands, and CABE (Analytical and Biophysical Environmental Chemistry), University of Geneva, Sciences II, 30 Quai E. Ansermet, Switzerland

In a previous study *(Langmuir* **2004**, *20*, 10324), the electrokinetic properties of *diffuse soft layers* were theoretically investigated within the framework of the Debye−Hückel approximation valid in the limit of sufficiently low values for the Donnan potential. In the current paper, the electrokinetics is tackled on the basis of the rigorous nonlinearized Poisson−Boltzmann equation, the numerical evaluation of the electroosmotic velocity profile, and the analytically derived hydrodynamic velocity profile. The results are illustrated and discussed for a diffuse soft interface characterized by a linear gradient for the friction coefficient and the density of hydrodynamically immobile ionogenic groups in the transition region separating the bulk soft layer and the bulk electrolyte solution. In particular, it is shown how the strong asymmetry for the potential distribution, as met for high values of the bulk fixed charge density and/or low electrolyte concentrations, is reflected in the electrokinetic features of the diffuse soft layer. The analysis clearly highlights the shortcomings of the discontinuous approximation by Ohshima and others for the modeling of the friction and electrostatic properties of soft layers exhibiting high Donnan potentials. This is in line with reported electrokinetic measurements of various soft particles and permeable gels at low electrolyte concentrations which fail to match predictions based on Ohshima's theory.

1. Introduction

Major efforts have been invested in the theoretical investigation of the electrokinetic properties of soft materials such as gels, polyelectrolyte-coated particles, or polyelectrolytes.[1−4] These studies are motivated by the increasing number of electrokinetic analyses aimed at the electrical, chemical, and hydrodynamic characterization of microorganisms[5] or three-dimensional polymer networks.[6−8] The theories so far proposed are based on the Poisson−Boltzmann equation for the electric potential distribution across the soft interface and the Navier−Stokes equation for the liquid flow velocity inside and outside the soft surface layer. More specifically, as far as the electrostatics are concerned, the concept of the Donnan potential has gained some consensus.[9] This concept underlies the assumption of electroneutrality in the bulk of the soft layer, as met by the charge balance between mobile ions stemming from the electrolyte solution and the hydrodynamically fixed (charged) ionogenic groups of the polymer segments. The hydrodynamics is treated within the framework of the Debye−Bueche model,[10]

which considers those polymer segments as resistance centers that exert frictional forces on the liquid flowing in the soft layer.

The above theories have in common that the volume fraction of polymer segments (ϕ), the density of fixed charges in the porous layer (ρ_{fix}), and the coefficient modeling the friction to hydrodynamic flow (k) are constant in the soft surface layer and drop sharply to zero at the very interface formed with the electrolyte side. In the first part of this series,[1] the step-function type modeling of the interface was abandoned and the term *diffuse soft interface* was introduced, stressing that continuous spatial profiles for ϕ, ρ_{fix}, and k across the interphasial region are explicitly taken into account. The motivation for evoking spatial gradual transition for these parameters was extensively discussed in ref 1, and the reader is referred to that paper for more details and further references. As a first-order approximation, a linear gradient for ϕ was considered in the diffuse interface, between bulk electrolyte solution and bulk soft layer. Assuming that the distribution of charged sites along the polymer segments is uniform, the spatial profile for the fixed charge density ρ_{fix} follows that of ϕ. The analysis was carried out for hydrogel layers with high water content. For such gels, there is a linear relationship between the friction coefficient k and the volume density ϕ, as expressed by the Stokes equation or equivalently the Brinkman equation in the limit of low ϕ,[11] so that k may be represented by a spatial profile similar to that for ϕ. Taking into account the position dependence of ρ_{fix} and k, electrostatic, hydrodynamic, and electroosmotic features were analytically solved for the (low potential) Debye−Hückel regime, within the context of streaming potential/streaming current. The analysis demonstrates how the coupled spatial distributions of the hydrodynamic and electrostatic parameters affect the electrokinetic properties of the soft layer, especially in

* E-mail*:* jerome.duval@wur.nl. Tel*:* 00 41 22 3796 429. Fax*:* 41 22 3796069.

(1) Duval, J. F. L.; van Leeuwen, H. P. *Langmuir* **2004**, *20*, 10324.

(2) Ohshima, H. *Adv. Colloid Interface Sci.* **1995**, *62*, 189.

(3) Hoogeveen, N. G.; Cohen Stuart, M. A.; Fleer, G. J. *Langmuir* **1996**, *12*, 3675.

(4) Fleer, G. J.; Cohen Stuart, M. A.; Scheutjens, J. M. H. M.; Cosgrove, T.; Vincent, B. In *Polymer at interfaces*; Chapman & Hall: London, 1993.

(5) Van der Wal, A., Ph.D. Thesis, Wageningen University, The Netherlands, 1996.

(6) Starov, V.; Solomentsev, Y. E. *J. Colloid Interface Sci.* **1993**, *158*, 159.

(7) Starov, V.; Solomentsev, Y. E. *J. Colloid Interface Sci.* **1993**, *158*, 166.

(8) Donath, E.; Voigt, A. *J Colloid Interface Sci.* **1986**, *109*, 122.

(9) Donath, E.; Pastuschenko, V. *Bioelectrochem. Bioenerg.* **1980**, *7*, 31.

(10) Debye, P.; Bueche, A. *J. Chem. Phys.* **1948**, *16*, 573.

(11) Brinkman, H. C. *Research* **1949**, *2*, 190.
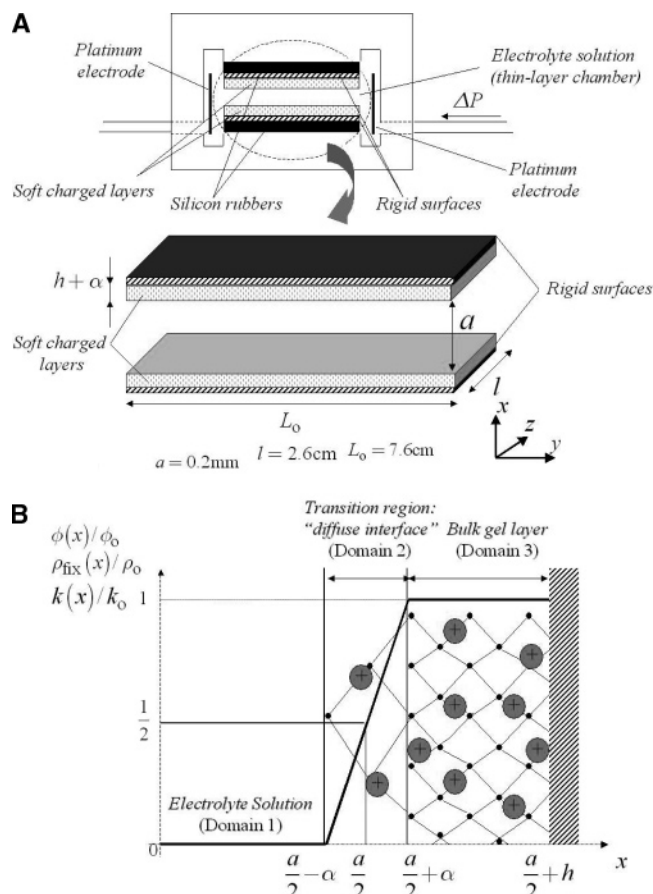
Figure 1. (A) Schematic representation of the experimental setup for streaming potential/streaming current measurements. The cell dimensions are indicated. (B) Spatial modeling adopted for the diffuse soft interface.

the low electrolyte concentration range (still compatible with the Debye–Hückel approximation) where the assumption of a diffuse nature of the interphase is crucial. Qualitatively, the results are consistent with experimental data at low electrolyte concentrations which do not merge with predictions derived from step-function modeling of the interface.[12–15]

In this paper, we propose to extend and generalize the electrokinetic theory of diffuse soft layers by taking the nonlinearized Poisson–Boltzmann equation. Particular attention will therefore be paid to the situation at low electrolyte concentrations and/or high densities of fixed charged groups, i.e., for diffuse soft interfaces characterized by high Donnan potentials. The electrokinetic properties are analyzed within the framework of streaming current/streaming potential of gel layers placed in a thin-layer cell of which the characteristic sizes (width l, length L_o, and height a) and arrangement are given in Figure 1A. The Cartesian coordinate system chosen is also represented. A pressure gradient $\Delta P/L_o$ is applied along the thin-layer chamber in the cell (y-axis). Two electrodes placed at the extremities of the chamber allow measurement of the current (streaming current) or lateral potential

(12) Makino, K.; Yamamoto, S.; Fujimoto, K.; Kawaguchi, H.; Ohshima, H. *J. Colloid Interface Sci.* **1994**, *166*, 251.
(13) Ohshima, H.; Makino, K.; Kato, T.; Fujimoto, K.; Kondo, T.; Kawaguchi, H. *J. Colloid Interface Sci.* **1993**, *159*, 512.
(14) Yezek, L.; Duval, J. F. L.; van Leeuwen, H. P. Submitted to *Langmuir*.
(15) Garcia-Salinas, M. J.; Romero-Cano, M. S.; de Las Nieves, F. J. *J. Colloid Interface Sci.* **2001**, *241*, 280.

difference (streaming potential) produced by the flow.[16] In Figure 1B, a schematic representation of the modeling for the diffuse soft interface, as discussed above and adopted within this study, is given. A flat and smooth surface represents the inner boundary of the layer and is considered to be uncharged. α stands for the characteristic thickness of the transition layer at the diffuse interface. ϕ_o, ρ_o, and k_o are the bulk values for the volume fraction of polymer segments, the charge density of fixed charged groups, and friction coefficient, respectively, in the gel layer of total thickness $h + \alpha$.

2. Electrostatics: Determination of the Potential Distribution across the Diffuse Interface

2.1. Solution to the Nonlinearized Poisson–Boltzmann Equation. The electric potential $\psi(x)$ inside and outside the diffuse soft layer is related to the charge density by the one-dimensional Poisson equation

$$\frac{d^2\psi(x)}{dx^2} = -\frac{\rho_{\text{fix}}(x) + \rho_{\text{el}}(x)}{\epsilon_o\epsilon} \tag{1}$$

where ϵ_o is the dielectric permittivity of vacuum and $\epsilon_o\epsilon$ is the dielectric permittivity of water. $\rho_{\text{el}}(x)$ is the local charge density of the mobile electrolyte ions, and $\rho_{\text{fix}}(x)$ is that of the fixed charges distributed in the soft layer as shown in Figure 1B. It is assumed that the dielectric permittivity in the bulk gel and in the diffuse interface equals that of water. This is a reasonable assumption for gel layers with sufficiently high water content, as considered here. Though differences in ion valencies may be easily accounted for, we treat here the case of an ion-penetrable structure immersed in a 1:1 electrolyte of bulk concentration n_∞. At equilibrium, the distribution of electrolyte ions across the interface obeys the Boltzmann statistics so that $\rho_{\text{el}}(x)$ may be written in the form

$$\rho_{\text{el}}(x) = -2en_\infty \sinh(y(x)) \tag{2}$$

with e the elementary charge and $y(x) \equiv F\psi(x)/RT$ the dimensionless potential (F is the Faraday, R the gas constant, and T the absolute temperature). Substituting eq 2, eq 1 becomes

$$\frac{d^2y(x)}{dx^2} - \kappa^2 \sinh(y(x)) = -\frac{e}{\epsilon_o\epsilon k_B T}\rho_{\text{fix}}(x) \tag{3}$$

where κ is the characteristic reciprocal Debye length defined by

$$\kappa = \left(\frac{2n_\infty e^2}{k_B T\epsilon_o\epsilon}\right)^{1/2} \tag{4}$$

with k_B the Boltzmann constant. The boundary conditions associated with eq 3 are of Dirichlet and Neumann types. They express the continuity of the electric potential and electric field at the positions $x = a/2 \pm \alpha$, that is

$$y(x)|_{(a/2-\alpha)^-} = y(x)|_{(a/2-\alpha)^+} \tag{5a}$$

$$\left.\frac{dy(x)}{dx}\right|_{(a/2-\alpha)^-} = \left.\frac{dy(x)}{dx}\right|_{(a/2-\alpha)^+} \tag{5b}$$

(16) Van Wagenen, R. A.; Andrade, J. D. *J. Colloid Interface Sci.* **1980**, *76 (2)*, 305.

$$y(x)|_{(a/2+\alpha)^-} = y(x)|_{(a/2+\alpha)^+} \tag{6a}$$

$$\left.\frac{dy(x)}{dx}\right|_{(a/2+\alpha)^-} = \left.\frac{dy(x)}{dx}\right|_{(a/2+\alpha)^+} \tag{6b}$$

Besides, the electric potential distribution should comply with the conditions of zero electric field at $x \gg a/2 + \alpha + \kappa^{-1}$ and $x \ll a/2 - \alpha - \kappa^{-1}$, i.e.

$$\left.\frac{dy(x)}{dx}\right|_{x\gg a/2+\alpha+\kappa^{-1}} = 0 \tag{7a}$$

$$y|_{x\gg a/2+\alpha+\kappa^{-1}} = \text{constant} = y^D \tag{7b}$$

and

$$\left.\frac{dy(x)}{dx}\right|_{x\ll a/2-\alpha-\kappa^{-1}} = 0 \tag{8a}$$

$$y|_{x\ll a/2-\alpha-\kappa^{-1}} = 0 \text{ (choice of the reference)} \tag{8b}$$

where y^D is the (dimensionless) Donnan potential. Using eqs 3 and 7, y^D is simply given by

$$y^D = \sinh^{-1}\left(\frac{\rho_o}{2en_\infty}\right) \tag{9}$$

Conditions 7 and 8 are valid providing there is no overlap of the double layers in the thin-layer cell, i.e., $\kappa a \gg 1$ and that the Donnan potential is effectively reached in the bulk gel layer, i.e., $\kappa h \gg 1$. These two situations are commonly met in practice.[14] Let us now consider separately the domains corresponding to the electrolyte solution (domain 1), the diffuse interface (domain 2), and the bulk gel layer (domain 3), as indicated in Figure 1B.

In domain 1, eq 3 is written

$$\frac{d^2y(x)}{dx^2} - \kappa^2 \sinh(y(x)) = 0 \tag{10}$$

Differential eq 10 may be integrated after multiplying both sides by $2dy/dx$. As

$$2\frac{dy}{dx}\frac{d^2y}{dx^2} = \frac{d(dy/dx)^2}{dx} \tag{11}$$

and

$$2\frac{dy}{dx}\sinh(y(x)) = 2\frac{d\cosh(y(x))}{dx} \tag{12}$$

first integration of eq 10 yields

$$\left[\frac{dy(x)}{dx}\right]^2 = 2\kappa^2\{\cosh(y(x)) + C\} \tag{13}$$

Using eq 8, we find for the integration constant $C = -1$. After separation and straightforward change of variables, the second integration provides

$$y(x) =$$
$$2\ln\left\{\frac{1 + \exp(y_m/2) + \exp[\kappa(x - a/2 + \alpha)][\exp(y_m/2) - 1]}{1 + \exp(y_m/2) - \exp[\kappa(x - a/2 + \alpha)][\exp(y_m/2) - 1]}\right\} \tag{14}$$

where $y_m = y(x = a/2 - \alpha)$. An expression for the electric field follows directly from eq 13 and we have particularly

$$\left.\frac{dy(x)}{dx}\right|_{x=a/2-\alpha} = 2\kappa \sinh(y_m/2) \tag{15}$$

In domain 3, the Poisson–Boltzmann equation (3) comes to

$$\frac{d^2y(x)}{dx^2} - \kappa^2 \sinh(y(x)) = -\kappa^2 \sinh(y^D) \tag{16}$$

Adopting the strategy aforementioned, after multiplication of both sides by $2dy/dx$ and exploitation of the boundary condition (7), first integration of eq 16 is written

$$\left[\frac{d\tilde{y}(x)}{dx}\right]^2 + 2\kappa^2\{\sinh(y^D)[\sinh(\tilde{y}(x)) - \tilde{y}(x)] - 2\cosh(y^D)[\sinh(\tilde{y}(x)/2)]^2\} = 0 \tag{17}$$

with $\tilde{y}(x) = y^D - y(x)$. Equation 17 may be rewritten in the form of an implicit transcendental integral equation in terms of the potential $y(x)$. After some rearrangements, one obtains

$$\int_{\sinh((y^D-y_p)/2)}^{\sinh((y^D-y(x))/2)} d\xi/\{[\cosh(y^D)]^{1/2}(1 + \xi^2)^{1/2} \times [\xi^2 - \tanh(y^D)\{\xi(1 + \xi^2)^{1/2} - \ln[\xi + (1 + \xi^2)^{1/2}]\}]^{1/2}\} = -\kappa(x - a/2 - \alpha) \tag{18}$$

where ξ is a dummy integration variable and $y_p = y(x = a/2 + \alpha)$. An expression for the electric field may be derived from eq 17. In particular we have

$$\left.\frac{dy(x)}{dx}\right|_{x=a/2+\alpha} = 2^{1/2}\kappa\left\{2\cosh(y^D)\left[\sinh\left(\frac{y^D - y_p}{2}\right)\right]^2 + \sinh(y^D)\{y^D - y_p - \sinh(y^D - y_p)\}\right\}^{1/2} \tag{19}$$

In domain 2, the Poisson–Boltzmann equation may be written as follows

$$\frac{d^2y(u)}{du^2} - (\kappa\alpha)^2\left\{\sinh(y(u)) + \frac{u}{2}\sinh(y^D)\right\} = 0 \tag{20}$$

with u the space variable defined by

$$u = 1 + \frac{x - a/2}{\alpha} \tag{21}$$

Unfortunately, there is no simple explicit expression for the electric field (first integration of eq 20) and for the potential distribution (second integration of eq 20) in the diffuse region of the gel/electrolyte solution interface. Therefore we developed a numerical algorithm to find the unique physical solution satisfying eq 20 under boundary conditions (5) and (6). For that purpose, the space variable u is written
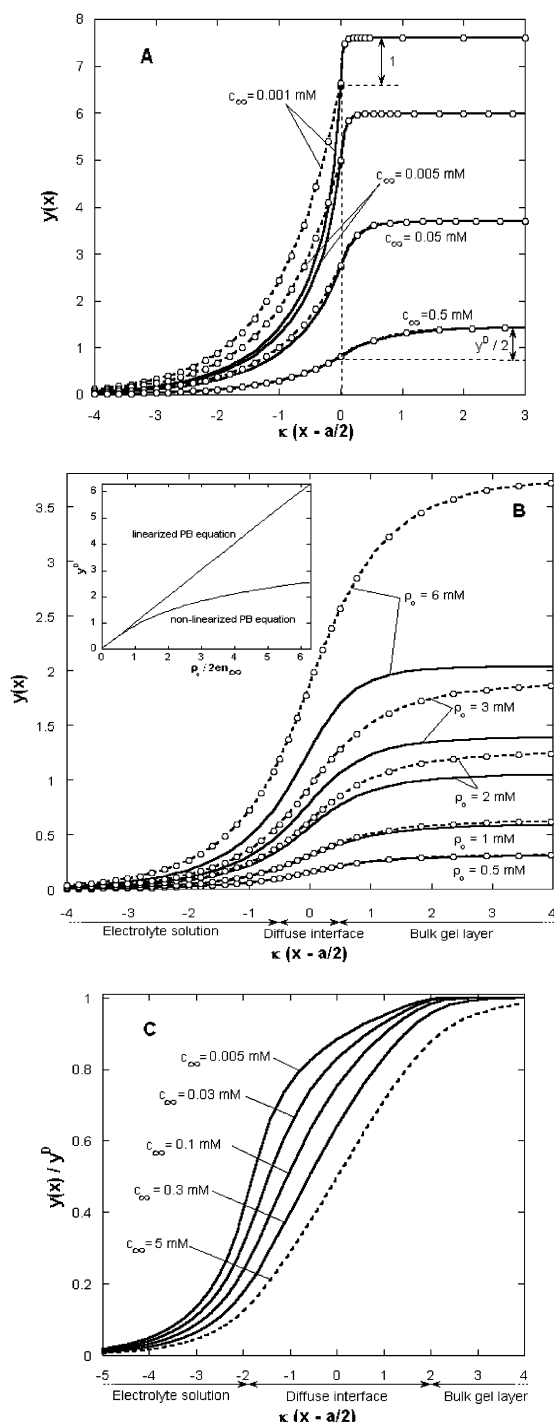
$$i \in [0, M]:$$

$$u_i = i\Delta u \tag{22}$$

with Δu the iteration step given by $\Delta u = 2/M$ where M is an integer. The discretized form of eq 20 is therefore

$$i \in [1, M - 1]:$$

$$\frac{y_{i+1} - 2y_i + y_{i-1}}{\Delta u^2} - (\kappa\alpha)^2\left\{\sinh(y_i) + i\frac{\Delta u}{2}\sinh(y^D)\right\} = 0 \tag{23}$$

Figure 2. (A) Potential distribution across the electrolyte solution/gel layer interface at different (1:1) electrolyte concentrations c_∞ (indicated). The numerical results (plain lines) are compared with the profiles obtained from the analytical expressions (eqs 26−29) (points + dashed curves). Model parameters: $\kappa\alpha = 0$ (step-function modeling for the interface), $\rho_o = 2$ mM. (B) Potential distribution across the diffuse interface electrolyte solution/gel layer as a function of the bulk fixed charges density ρ_o (indicated). The numerical results (solid lines) are compared with the analysis based on the linearization of the Poisson−Boltzmann equation[1] (points + dashed curves). In inset, the discrepancies between y^D values as calculated within the framework of the Debye−Hückel approximation[1] and from the full nonlinearized Poisson−Boltzamnn equation (this study) are illustrated. Model parameters: $c_\infty = 0.8$ mM, $\kappa\alpha = 1/2$. (C) Normalized potential profiles $y(x)/y^D$ across a diffuse soft interface as a function of c_∞ (indicated). $\rho_o = 2$ mM, $\kappa\alpha = 2$. Numerical results, solid lines; prediction from linear analysis,[1] dashed curve.

with $y_i = y(u = u_i)$. The boundary conditions (5) and (6) may be expressed by means of the analytical equations (15) and (19) valid at the borders of domain 2. One obtains

$$\frac{y_1 - y_0}{\Delta u} = 2\kappa\alpha \sinh(y_0/2) \tag{24}$$

$$\frac{y_M - y_{M-1}}{\Delta u} = 2^{1/2}\kappa\alpha\left\{2\cosh(y^D)\left[\sinh\left(\frac{y^D - y_M}{2}\right)\right]^2 + \sinh(y^D)\{y^D - y_M - \sinh(y^D - y_M)\}\right\}^{1/2} \tag{25}$$

The nonlinear system consisting of the $M + 1$ equations (23−25) has the $M + 1$ potentials, $y_{i=0...M}$, as the only unknown variables. This system was solved consistently using a Newton−Raphson type algorithm.[17] In particular the values of $y_0 = y(x = a/2 - \alpha) \equiv y_m$ and $y_M = y(x = a/2 + \alpha) \equiv y_p$ were found so that the potential distributions in domain 1 and domain 3 follow directly from eq 14 and numerical evaluation of the integral eq 18, respectively. At this stage of the analysis, the potential distribution across the interface as depicted in Figure 1B is completely determined. In passing, we note that computation of the potential distribution across the diffuse interface may of course be performed by systematic discretization of the Poisson−Boltzmann equation in domains 1, 2, and 3. This method, less elegant than that proposed above, provides lesser accurate results because of the necessary larger step size to cover the whole x-range of interest.

2.2. Results and Discussion. For the sake of validation of the numerical method, in Figure 2A we first give potential profiles as calculated for $\alpha = 0$ at various electrolyte concentrations $c_\infty = n_\infty/N_a$ (N_a Avogadro number) and fixed ρ_o. This situation corresponds to the classical step-function-type modeling of the interface as first proposed by Ohshima who derived the following approximate analytical expressions for the potential[18]

$$y(x) = y^o \exp[\kappa(x - a/2)] \quad (x < a/2) \tag{26}$$

$$y(x) = y^D + (y^o - y^D)\exp[-\kappa_m(x - a/2)] \quad (x > a/2) \tag{27}$$

where y^o is the sometimes called "surface potential", i.e., the potential at $x = a/2$ defined by[18]

$$y^o = y^D - \tanh(y^D/2) \tag{28}$$

and κ_m represents the typical characteristic reciprocal decay length of the potential in the gel layer

$$\kappa_m = \kappa[\cosh(y^D)]^{1/2} \tag{29}$$

Equations 26 and 27 follow from the linearization and subsequent integrations of the Poisson−Boltzmann equation with respect to the quantities $y(x)$ and $y^D - y(x)$, respectively. For high c_∞ (i.e., low y^D, see eq 9), the predictions based on the analytical equations (26−29) very well match the potential distribution as calculated from the numerical procedure outlined in the previous section. In particular, the potential profile $y(x)$ is antisymmetric around the point of coordinates $(x = a/2, y^o \to y^D/2)$, the

(17) Press: W. H.; Teukolsky, S. A.; Vetterling, W. T.; Flannery, B. P. In *Numerical Recipes in Fortran, The art of Scientific Computing*, 2nd ed.; Cambridge University Press: Cambridge, U.K., 1986.

(18) Ohshima, H.; Kondo, T. *Biophys. Chem.* **1990**, *38*, 117.
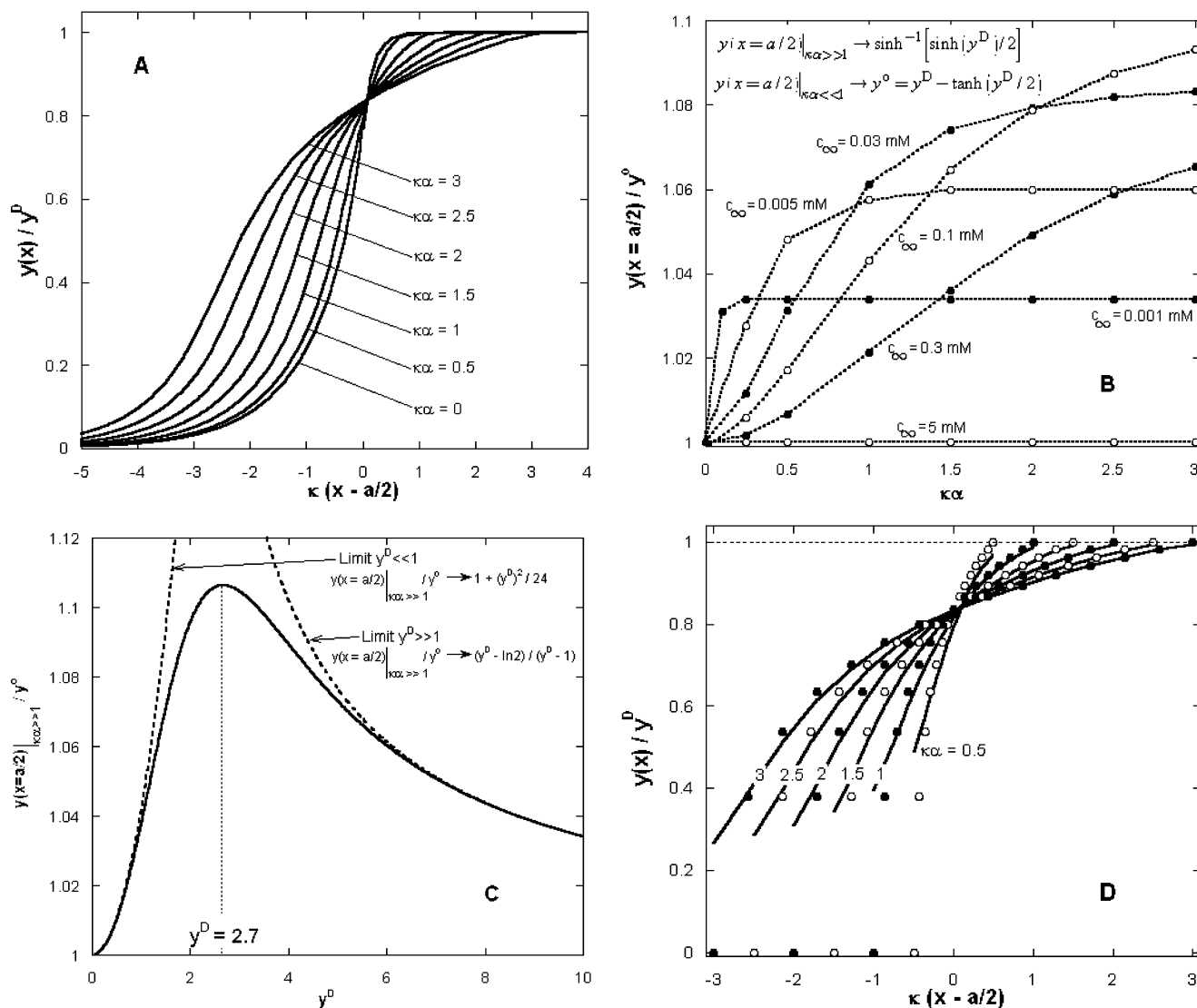
Figure 3. (A) Illustration of the effect of the thickness of the diffuse interface, expressed in terms of $\kappa\alpha$ (indicated), on the (normalized) potential distribution. Other parameters: $c_\infty = 0.03$ mM, $\rho_o = 2$ mM ($y^D = 4.2$). (B) Dependencies of the ratio $y(x = a/2)/y^o$ (y^o defined by expression 28) on the electrolyte concentration c_∞ (indicated) and $\kappa\alpha$. Other parameters, as in panel A. (C) Ratio $y(x = a/2)|_{\kappa\alpha\gg1}/y^o$ (expressions 28 and 31) as a function of the Donnan potential y^D. The dashed curves represent the behavior at low and large y^D. The corresponding analytical expressions are given. (D) Comparison between numerical results (solid lines) and analytical expression (eq 30) (points) for the potential distribution in domain 2 as a function of $\kappa\alpha$ (indicated). Other parameters, as in panel A.

space charge layer thickness (κ_m^{-1}) in the gel equating that in the solution (κ^{-1}) (see eq 29). Upon decrease of c_∞ (that is, with increasing y^D) the antisymmetry gradually disappears in accordance with eqs 27–29. Deviations between numerical and analytical results are observed for $x < a/2$, the region where the Debye–Hückel approximation used to derive eq 26 becomes invalid. In the limit of very dilute electrolytes, we find $y^o \to y^D - 1$, which is in line with eq 28. In panels B and C of Figure 2, we give the first numerical results pertaining to the case of a diffuse soft interface. The data are compared with the results derived on the basis of the analytical study presented in ref 1. Basically the same comments as for Figure 2A may be given. Upon increase of ρ_o (or decrease of c_∞) at constant c_∞ (ρ_o) and constant α, significant discrepancies between linear and nonlinear treatments of the Poisson–Boltzmann equation appear, as expected. These discrepancies refer not only to the magnitude of the total potential drop across the interface, i.e., y^D (panel B, Figure 2), but also to the asymmetric pattern exhibited

by the normalized potential distribution $y(x)/y^D$. Such asymmetry cannot be predicted when operating on the Debye–Hückel level (panel C, Figure 2).

In Figure 3, the effect of the thickness of the diffuse interface on the potential distribution *at high* y^D is analyzed in some more detail. Starting from the situation pertaining to a discontinuous segment distribution across the interface ($\kappa\alpha = 0$), the potential y decreases (increases) for $x > a/2$ ($x < a/2$) upon increase of $\kappa\alpha$. This is caused by the corresponding decrease (increase) of the local charge density of fixed charges, $\rho_{fix}(x)$. The pronounced asymmetry of the potential profiles across the diffuse interface is the result of the nonlinear coupling between the spatial functionalities for ρ_{fix} and ρ_{el} (see eq 1) which exhibit very different symmetry properties with respect to the position $x < a/2$ (see Figure 2A and Figure 1B). On closer inspection, the different curves reported in Figure 3A do not have a common intersection point because the potential $y(x = a/2)$ slightly depends on α. This is illustrated in Figure 3B where the effect of the electrolyte concentration on $y(x =$

$a/2$) is also indicated. To qualitatively understand the trends, let us first consider the situations where $\kappa\alpha \gg 1$. Neglecting the first term in the left-hand side of eq 20, one immediately obtains in domain 2 (diffuse region) the following analytical expression for the potential

$$y(x)|_{\kappa\alpha\gg1} \approx \sinh^{-1}\left\{\frac{1}{2}\sinh(y^D)\left(1 + \frac{x - a/2}{\alpha}\right)\right\} \quad (30)$$

so that

$$y(x = a/2)|_{\kappa\alpha\gg1} \rightarrow \sinh^{-1}\left\{\frac{1}{2}\sinh(y^D)\right\} \quad (31)$$

Besides we already know from eq 28 that

$$y(x = a/2)|_{\kappa\alpha\ll1} \rightarrow y^o = y^D - \tanh(y^D/2) \quad (32)$$

For intermediate values of $\kappa\alpha$, $y(x = a/2)$ increases from y^o to the limit given by expression 31, in agreement with the results of Figure 3B. The ratio $y(x = a/2)|_{\kappa\alpha\gg1}/y^o$ is plotted as a function of y^D in Figure 3C. The maximum predicted around $y^D \simeq 2.7$ is very well reproduced by the numerical analysis for different c_∞ (Figure 3B). In Figure 3D, comparison is made for various $\kappa\alpha$ between the numerically calculated potential distributions in domain 2 with those based on expression 30. It appears that deviations show up when decreasing x from the position $x = a/2$, as expected, but more interesting is the observation that eq 30 fits very well the numerical predictions in the region $a/2 < x \leq a/2 + \alpha$ not only for large values of $\kappa\alpha$ but also for intermediate ones ($\kappa\alpha \approx 1$). This is so because there the potential drop is either very steep (low κ_m^{-1}) or quasi-linear (see Figure 3A) so that the term d^2y/dx^2 in eq 20 rapidly vanishes upon increase of $\kappa\alpha$ thus rendering eq 30 into an excellent approximate expression for the potential in the aforementioned region. From eq 30, one also infers that $y(x = a/2 + \alpha)_{\kappa\alpha\gg1} = y_p|_{\kappa\alpha\gg1} = y^D$, in accordance with the numerical results. This effectively means that the electric field in the bulk gel layer is zero for large $\kappa\alpha$. In other words, the potential distribution in domain 3 and in the spatial range $a/2 < x \leq a/2 + \alpha$ (see previous comments) is determined predominantly by the spatial distribution of charges in the gel and to a much lesser extent by that of the mobile ions. This result is particularly important for the examination of electrokinetics of strongly swollen soft layers (situation classically met at high y^D or equivalently low c_∞) for which the typical thickness α may largely exceed the characteristic length scale(s) κ_m^{-1} and/or κ^{-1}. Obviously, modeling of the electrokinetics of such charged layers upon discontinuous approximation for the segment distribution is inappropriate (see section 5).

3. Hydrodynamics

3.1. Determination of the Flow Velocity Profile in the Thin-Layer Chamber. Determination of the flow velocity profile $v(x)$ inside and outside the diffuse soft layer is carried out on the basis of the Navier−Stokes equation. The analysis is performed in detail in ref 1, and we shall here only recall the approximations made and the conditions for which these are valid: (i) the hydrodynamic interactions are neglected, which is justified for the laminar flow regime (Reynolds number $Re < 2500$); (ii) hydrodynamics is time-independent, as assumed within the framework of the treatment of the electrostatics (no

transient processes taken into account); (iii) there is no overlap of the two parallel diffuse soft layers in the thin-layer cell; (iv) the friction properties of the surface layers are derived on the basis of Brinkman's equation[11] which relates the spatial distribution $\phi(x)$ with that for the friction coefficient k (see introduction); (v) gel layers with high water contents are considered (so that $k(x) \propto \phi(x)$). We also recall that the effect of the electrostatic interactions between ions from the solution and polymer segments on the rheological features of the gel layers are not included in Brinkman's equation. This aspect seems to deserve further consideration.

The mathematical treatment of the Navier Stokes equation within the approximations aforementioned is rather straightforward but tedious.[1] Profile $v(x)$ is axisymmetric around $x = 0$, and for domains 1, 2, and 3 one obtains the expressions

$0 \leq x \leq a/2 - \alpha$:

$$v(x) = -\frac{\Delta P}{2\eta_w L_o}x^2 + C_1 x + C_2 \quad (33)$$

$a/2 - \alpha \leq x \leq a/2 + \alpha$:

$$v(x) = v_0 + v_1 u(x) + v_2 [u(x)]^2 + \sum_{j=0}^{2}\sum_{n=1}^{\infty}\theta^n\frac{j!}{(3n+j)!}f(n,j)v_j[u(x)]^{3n+j} \quad (34)$$

with

$$f(n,j) = \prod_{p=0}^{n-1}(3p + j + 1) \quad (35)$$

and

$$\theta = \frac{(\alpha\lambda_o)^2}{2} \quad (36)$$

$a/2 + \alpha \leq x \leq a/2 + h$:

$$v(x) = \frac{\Delta P}{\eta_w L_o \lambda_o^{2}} + C_3 \exp\left[\frac{-x + (a/2 + \alpha)}{\lambda_o^{-1}}\right] + C_4 \exp\left[\frac{x - (a/2 + h)}{\lambda_o^{-1}}\right] \quad (37)$$

respectively. $\lambda_o^{-1} = (k_o/\eta_w)^{-1/2}$ (η_w dynamic viscosity of water) represents the hydrodynamic penetration length of the fluid in the bulk gel layer (λ_o is commonly called the softness parameter). The constant v_2 is defined by

$$v_2 = -\frac{\Delta P\alpha^2}{2\eta_w L_o} \quad (38)$$

and the position-independent terms $(C_i)_{1\leq i\leq 4}$, $(v_i)_{i=0,1}$ satisfy the system consisting of six linear equations derived from the boundary conditions associated with the Navier−Stokes equation. These boundaries reflect the continuity of $v(x)$ and $dv(x)/dx$ at $x = a/2 \pm \alpha$, stagnancy at $x = a/2 + h$, and symmetry of $v(x)$ with respect to $x = 0$. After some rearrangement, they are written as

$$C_1 = 0 \tag{39}$$

$$C_2 = v_0 + \frac{\Delta P}{2\eta_w L_o}\left(\frac{a}{2} - \alpha\right)^2 \tag{40}$$

$$v_1 = -\frac{\Delta P \alpha}{\eta_w L_o}\left(\frac{a}{2} - \alpha\right) \tag{41}$$

$$\frac{\Delta P}{\eta_w L_o \lambda_o^2} + C_3 + C_4 \exp[\lambda_o(\alpha - h)] -$$
$$\sum_{j=0}^{2} 2^j v_j\left(1 + \sum_{n=1}^{\infty} \theta^n \frac{2^{3n} j!}{(3n+j)!} f(n,j)\right) = 0 \tag{42}$$

$$(2\theta)^{1/2}(C_4 \exp[\lambda_o(\alpha - h)] - C_3) -$$
$$\sum_{j=0}^{2} v_j\left(j^2 + \sum_{n=1}^{\infty} \theta^n \frac{2^{3n+j-1} j!}{(3n+j-1)!} f(n,j)\right) = 0 \tag{43}$$

$$C_4 = -\left(\frac{\Delta P}{\eta_w L_o \lambda_o^2} + C_3 \exp[\lambda_o(\alpha - h)]\right) \tag{44}$$

3.2. Results and Discussion. The characteristic peculiarities of the profiles $v(x)$ were extensively discussed in ref 1. Here we only give results obtained for v at various values for α in the vicinity of $x = a/2$ so as to clearly highlight the effect of the position-dependent friction properties on the hydrodynamics (Figure 4) and in a latter stage (section 5) on the electrokinetics of surface layers with high Donnan potentials. The velocity is normalized with respect to the value reached in the bulk gel layer, that is, the quantity $\Delta P/\eta_w L_o \lambda_o^2$ (see eq 37). Upon increase of α, v decreases in the whole range of x as the result of (i) the corresponding increase of the friction coefficient $k(x \leq a/2)$ or equivalently the decrease of the hydrodynamic penetration length $\lambda^{-1}(x \leq a/2) = [k(x \leq a/2)/\eta_w]^{-1/2}$ and (ii) the decrease of the maximum velocity $v(x = 0)$ (not shown). With increasing k_o at constant α, $v(x)$ is reduced for every x, as expected, and the velocity gradient increases around the position $x = a/2 - \alpha$ (Figure 4). This is so because the diffuse model gradually approaches the limit of a step-function representation for the friction coefficient distribution across the interface.

4. Electroosmotic Velocity Profile

4.1. Numerical Analysis of the Navier−Stokes Equation Applied to the Diffuse Soft Interface. The streaming potential $\Delta\varphi_{str}$ is the potential difference at zero net current caused by the flow of liquid under the pressure gradient $\Delta P/L_o$ applied through the thin-layer cell. Under the action of the lateral electric field $\Delta\varphi_{str}/L_o$ on the countercharge located inside and outside the diffuse soft layer, an electroosmotic flow v_{eo} develops in the y-direction and is directed against the hydrodynamic flow. Here, we propose evaluation of the profile $v_{eo}(x)$ on the basis of the potential distribution as determined in section 2. $v_{eo}(x)$ derives from the Navier−Stokes equation for stationary flow in the incompressible limit

$$\frac{d^2 v_{eo}(x)}{dx^2} - [\lambda(x)]^2 v_{eo}(x) = -\Gamma E \sinh(y(x)) \tag{45}$$

with $\Gamma = 2en_\infty/\eta_w$, $E = \Delta\varphi_{str}/L_o$, and $\lambda^{-1}(x)$ the spatial distribution of the hydrodynamic penetration length as obtained from that of the friction coefficient. The boundary conditions pertaining to eq 45 are similar to those associated with the profile $v(x)$ (section 3), i.e., continuity
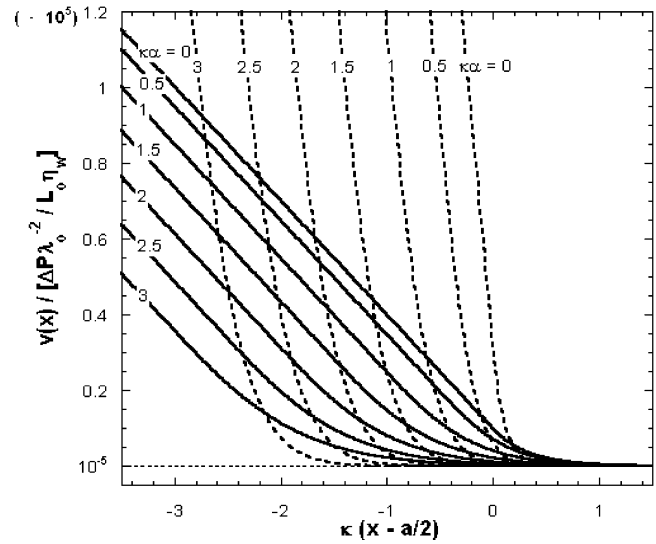
Figure 4. Hydrodynamic (dimensionless) velocity profiles for different values of $\kappa\alpha$ (indicated) and $\kappa\lambda_o^{-1} = 0.10$ (dashed lines) and $\kappa\lambda_o^{-1} = 0.33$ (solid lines). Model parameters: $c_\infty = 0.1$ mM, $a = 0.2$ mm, $h/a = 0.1$. For the sake of clarity, the profiles are drawn only in the vicinity of $x = a/2$.

of the velocity at $x = a/2 \pm \alpha$

$$v_{eo}(x)|_{(a/2-\alpha)^-} = v_{eo}(x)_{(a/2-\alpha)^+} \tag{46a}$$

$$\left.\frac{dv_{eo}(x)}{dx}\right|_{(a/2-\alpha)^-} = \left.\frac{dv_{eo}(x)}{dx}\right|_{(a/2-\alpha)^+} \tag{46b}$$

$$v_{eo}(x)|_{(a/2+\alpha)^-} = v_{eo}(x)_{(a/2+\alpha)^+} \tag{47a}$$

$$\left.\frac{dv_{eo}(x)}{dx}\right|_{(a/2+\alpha)^-} = \left.\frac{dv_{eo}(x)}{dx}\right|_{(a/2+\alpha)^+} \tag{47b}$$

stagnancy at $a/2 + h$

$$v_{eo}(x)|_{(a/2+h)} = 0 \tag{48}$$

and local symmetry with respect to $x = 0$

$$\left.\frac{dv_{eo}(x)}{dx}\right|_0 = 0 \tag{49}$$

In domain l (electrolyte solution), integration of eq 45 is straightforward. Using eq 10 and the boundary condition (49), one immediately obtains

$$v_{eo}(x) = v_{eo_m} - \frac{2\Gamma E}{\kappa^2} \times$$
$$\left\{\ln\left(\frac{1 + \exp(y_m/2) + \exp[\kappa(x - a/2 + \alpha)][\exp(y_m/2) - 1]}{1 + \exp(y_m/2) - \exp[\kappa(x - a/2 + \alpha)][\exp(y_m/2) - 1]}\right) - \frac{y_m}{2}\right\} \tag{50}$$

with $v_{eo} = v_{eo}(x = a/2 - \alpha)$, and

$$\left.\frac{dv_{eo}(x)}{dx}\right|_{x=a/2-\alpha} = -\frac{2\Gamma E}{\kappa}\sinh\left(\frac{y_m}{2}\right) \tag{51}$$

In domains 2 and 3, there are no simple analytical solutions to the corresponding Navier−Stokes equation. Therefore, we seek the numerical solution to the electroosmotic profile using the following discretization scheme

$i \in [1, M-1]$:

$$\frac{v_{eo_{i+1}} - 2v_{eo_i} + v_{eo_{i-1}}}{\Delta u^2} - 2\theta i \Delta u v_{eo_i} = -\Gamma E \alpha^2 \sinh(y_i) \tag{52}$$

in domain 2, with Δu and θ defined in eqs 22 and 36, respectively, and $v_{eo_i} = v_{eo}(u = u_i)$. The corresponding potentials y_i are already known (section 2). In domain 3, eq 45 takes the form

$j \in [1, N-1]$:

$$\frac{v_{eo_{j+1+M}} - 2v_{eo_{j+M}} + v_{eo_{j-1+M}}}{\Delta \tilde{x}^2} - (\kappa \lambda_o)^2 v_{eo_{j+M}} =$$
$$-\Gamma E \kappa^2 \sinh(y_{j+M}) \tag{53}$$

with N an integer, y_{j+M} the potentials as calculated using eq 18, $v_{eo_{j+M}}$ the corresponding electroosmotic velocities, and $\Delta \tilde{x}$ the step in the spatial domain 3 ($\tilde{x}_j = \kappa x_j = \kappa(a/2 + \alpha + j\Delta\tilde{x})$) defined by the relationship

$$\Delta \tilde{x} = \frac{r\kappa^{-1}}{N} \tag{54}$$

with $r \gg 1$ an integer such that

$$y(x \geq a/2 + \alpha + r\kappa^{-1}) = y^D \tag{55}$$

For $a/2 + \alpha + r\kappa^{-1} \leq x \leq a/2 + h$ ($dy/dx = 0$ and $y = y^D$), one can easily show that $v_{eo}(x)$ is simply given by the analytical expression

$$v_{eo}(x) = \frac{\Gamma E \sinh(y^D)}{\lambda_o^2} + D_1 \exp\left[\frac{-x + (a/2 + \alpha)}{\lambda_o^{-1}}\right] +$$
$$D_2 \exp\left[\frac{x - (a/2 + h)}{\lambda_o^{-1}}\right] \tag{56}$$

where D_1 and D_2 are obtained from the condition $v_{eo}(x = a/2 + \alpha + N\Delta\tilde{x}) = v_{eo_{N+M}}$ and the boundary (48), respectively, i.e.

$$D_1 = \frac{v_{eo_{N+M}} - \dfrac{\Gamma E \sinh(y^D)}{\lambda_o^2}\left\{1 - \exp\left[\dfrac{\alpha - h + N\Delta\tilde{x}}{\lambda_o^{-1}}\right]\right\}}{\exp(-N\lambda_o\Delta\tilde{x}) - \exp[2\lambda_o(\alpha - h) + N\Delta\tilde{x}]} \tag{57}$$

$$D_2 = -\left\{\frac{\Gamma E \sinh(y^D)}{\lambda_o^2} + D_1 \exp[\lambda_o(\alpha - h)]\right\} \tag{58}$$
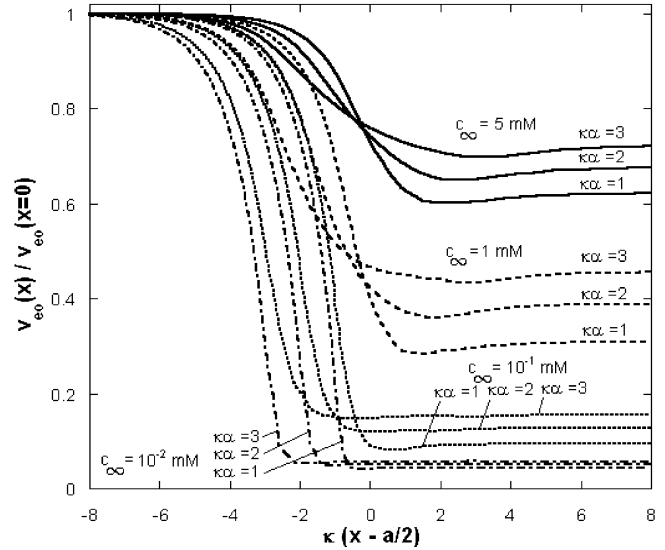
Besides, we have

$$\frac{dv_{eo}(x)}{dx}\Big|_{x_N} = \lambda_o D_1 \exp(\lambda_o N\Delta\tilde{x}) +$$
$$\lambda_o D_2 \exp[\lambda_o(\alpha - h + N\Delta\tilde{x})] \tag{59}$$

Using eq 51, boundary condition (46) is written

$$\frac{-v_{eo_2} + 4v_{eo_1} - 3v_{eo_0}}{2\Delta u} = -\frac{2\Gamma\alpha E}{\kappa}\sinh\left(\frac{y_m}{2}\right) \tag{60}$$

where a forward difference approximation with second error is employed for expressing the first derivative

Figure 5. Electroosmotic velocity profiles (normalized with respect to $v_{eo}(x = 0)$) as a function of $\kappa\alpha$ and c_∞ (indicated). $a = 0.2$ mm, $h/a = 0.01$, $\rho_o = 1$ mM, $\lambda_o^{-1} = 4.5$ nm.

$dv_{eo}(x)/dx$ at $x = a/2 - \alpha$, and $v_{eo_0} = v_{eo_m}$. Condition 47 is simply

$$\frac{3v_{eo_M} - 4v_{eo_{M-1}} + v_{eo_{M-2}}}{\Delta u} = \kappa\alpha \frac{-v_{eo_{M+2}} + 4v_{eo_{M+1}} - 3v_{eo_M}}{\Delta\tilde{x}} \tag{61}$$

where backward and forward approximations with second order are considered for the first derivative of v_{eo} at the positions $x = (a/2 + \alpha)^-$ (left-hand side) and $x = (a/2 + \alpha)^+$ (right-hand side), respectively. Furthermore, the profile should satisfy the conditions reflecting the continuity of $v_{eo}(x)$ and $dv_{eo}(x)/dx$ at the position x_N, that is

$$\frac{3v_{eo_{M+N}} - 4v_{eo_{M+N-1}} + v_{eo_{M+N-2}}}{2\Delta\tilde{x}} =$$
$$\frac{\lambda_o}{\kappa}\{D_1(v_{eo_{N+M}}) \exp(\lambda_o N\Delta\tilde{x}) +$$
$$D_2(v_{eo_{N+M}}) \exp[\lambda_o(\alpha - h + N\Delta\tilde{x})]\} \tag{62}$$

where we have used expression 59. D_1 and D_2 are two functions of $v_{eo_{N+M}}$ which comply with relations 57 and 58. The system consisting of the $N + M + 1$ linear equations (52, 53, 60−62) has the $N + M + 1$ velocities $v_{eo_{0,...N+M}}$ as unknown variables. This system was solved consistently using classical linear algebra machinery.[17] Subsequently, the profile $v_{eo}(x)$ in the spatial regions corresponding to domain 1 and to the domain $a/2 + \alpha + r\kappa^{-1} \leq x \leq a/2 + h$ were obtained using eqs 50 and 56, respectively. As for the treatment of the Poisson−Boltzmann equation (section 2), the (semi-) numerical analysis of the Navier−Stokes equation yields convergence of the solutions within very short computation time and a restricted number of iterations. The errors made in the finite difference schemes applied to eq 45 are of the order $O(\Delta u^2)$ and $O(\Delta\tilde{x}^2)$ for domain 2 and domain 3, respectively.

4.2. Results and Discussion. Figure 5 depicts typical profiles obtained for $v_{eo}(x)$ as a function of bulk electrolyte concentration, c_∞, and thickness of the diffuse interface expressed in terms of the dimensionless quantity, $\kappa\alpha$. In the regime of low Donnan potentials y^D (high electrolyte concentration), the numerical results are in very good agreement with those derived on the basis of the linearized
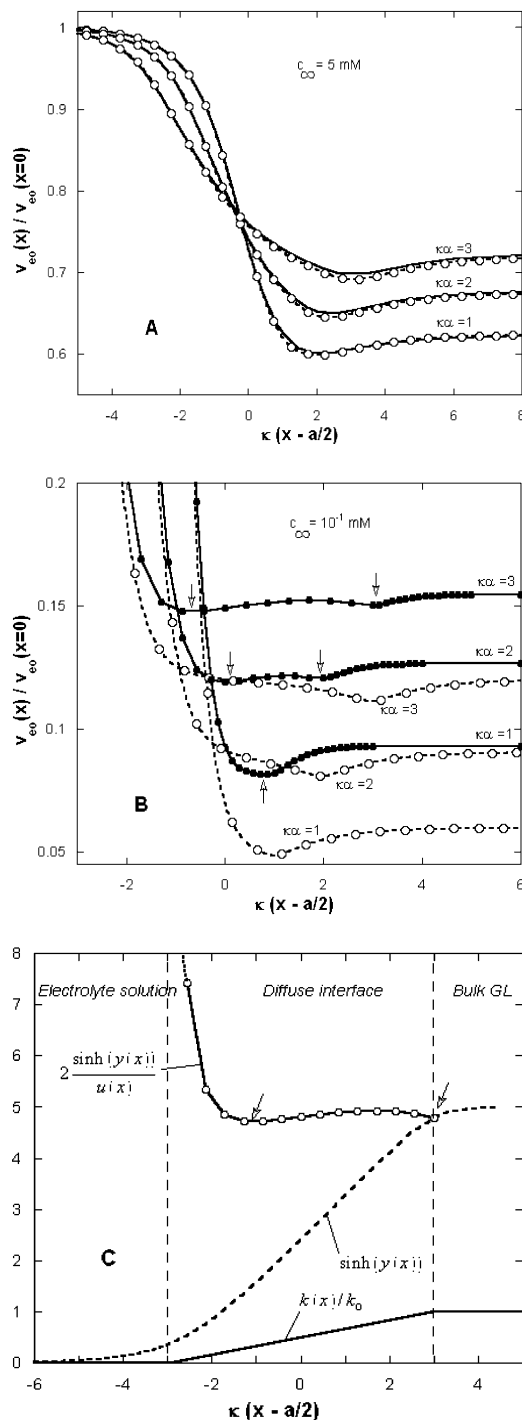
Figure 6. (A) Comparison between numerically (solid lines) and analytically[1] (points + dashed curves) computed electro-osmotic velocity profiles for $c_\infty = 5$ mM, $\rho_o = 1$ mM ($y^D = 0.1$). (B) The same as in panel A but for $c_\infty = 0.1$ mM and $\rho_o = 1$ mM ($y^D = 2.3$). The arrows indicate the minima exhibited by the profiles obtained from numerical analysis of the electrokinetic equations. For (A) and (B), $a = 0.2$ mm, $h/a = 0.01$, $\lambda_o^{-1} = 4.5$ nm. (C) Graphical representation of the balance between electrostatic and hydrodynamic effects (see text), which explains the origin of the two minima for the profiles $v_{eo}(x)$ at large $\kappa\alpha$ and low electrolyte concentration (marked with arrows). Model parameters: $\kappa\alpha = 2$, $c_\infty = 0.1$ mM.

Poisson−Boltzmann/Navier−Stokes equations,[1] as illustrated in Figure 6A. In particular, the increase (decrease) of the normalized electroosmotic velocity $v_{eo}(x)/v_{eo}(x=0)$ for $x \geq a/2 (x \leq a/2)$ upon increase of $\kappa\alpha$, as the result of the corresponding decrease (increase) of the

local friction coefficients, is very well reproduced. So are the slight decrease of $v_{eo}(x=0)$, as due to a broader spatial range for k, and the presence of a minimum for $x \geq a/2 + \alpha$. The physics behind that minimum was already discussed in ref 1. Basically, it originates from the shift in positions from which the bulk friction properties (k_o) and bulk electrostatics (y^D) are reached in the gel layer. The reader is referred to ref 1 for further detail. When decreasing c_∞ at given $\kappa\alpha$, the electroosmotic velocity $v_{eo}(x = 0)$ in the bulk electrolyte, given by

$$v_{eo}(x = 0) = v_{eo_m} + \epsilon_o\epsilon E k_B T y_m/e\eta_w \qquad (63)$$

considerably increases due to the sharp rise in the potentials $y(x)$, as shown in Figure 2C, and the concomitant increase in countercharge density. Since the electroosmotic velocity in the bulk gel layer, defined by

$$v_{eo}(x \gg a/2 + \alpha + \kappa_m^{-1}) = \frac{\rho_o E}{\eta_w \lambda_o^2} \qquad (64)$$

remains independent of c_∞, the profile $v_{eo}(x)/v_{eo}(x=0)$ drops steeply at the electrolyte side of the interface when lowering c_∞. Besides, the dependence of v_{eo} on position spans over broader/shorter ranges at the electrolyte/bulk gel layer sides, respectively. This is so because $\kappa^{-1}/\kappa_m^{-1}$ increases/decreases respectively, upon decrease of c_∞.

Let us now consider in more detail the effect of $\kappa\alpha$ on the profiles $v_{eo}(x)$ in the diffuse part of the interface at low c_∞ (Figure 6B). For low $\kappa\alpha$ ($\kappa\alpha \approx 1$), $v_{eo}(x)$ exhibits a minimum around $x \approx a/2 + \alpha$. The explanation is similar to that given for large c_∞ (ref 1, Figure 6A). Starting from a position x_o such that $x_o > a/2 + \alpha$, the potential distribution $y(x)$ (or equivalently the density of mobile charges $\rho_{el}(x)$) slightly decreases when reducing x down to $a/2 + \alpha$ whereas the friction coefficient remains constant so that $v_{eo}(x)$ decreases (electrostatic effect). Upon further decrease of x, decrease of k compounds the decrease in the potential so that $v_{eo}(x)$ increases (hydrodynamic effect). For larger values of $\kappa\alpha$, besides that first minimum, a second minimum positioned at $x < a/2 + \alpha$ emerges. The presence of that second minimum is again attributed to a subtle balance between electrostatic and hydrodynamic characteristics of the diffuse soft layer. A way to quantitatively appreciate this balance is to derive an analytical expression for $v_{eo}(x)$ in domain 2 at large $\kappa\alpha$. From eq 45, one immediately infers in the limit $\kappa\alpha \gg 1$

$$v_{eo}(x) \approx \frac{2en_\infty E \sinh(y(x))}{\eta_w \lambda_o^2 u(x)} \qquad (65)$$

where one recognizes that the numerator and denominator of the ratio at the right-hand side stand for the electrostatic and hydrodynamic components to the electroosmotic velocity, respectively. Expression 65 is plotted in Figure 6C as a function of the position. The two minima previously mentioned are clearly marked at $x \approx a/2 + \alpha$ and $x < a/2 + \alpha$. Furthermore, comparison of the (dimensionless) profiles as obtained from numerical analysis and linearization of the Poisson−Boltzmann/Navier−Stokes equation (Figure 6B) reveals that the presence of the second minimum is a direct consequence of the strong asymmetry of the potential profiles at large $\kappa\alpha$ and low c_∞ (see Figure 2C). When decreasing the friction coefficient k_o while maintaining all other parameters constant, the profiles $v_{eo}(x)$ are shifted upward, as expected, and the dependence on $\kappa\alpha$ gradually vanishes (not shown).
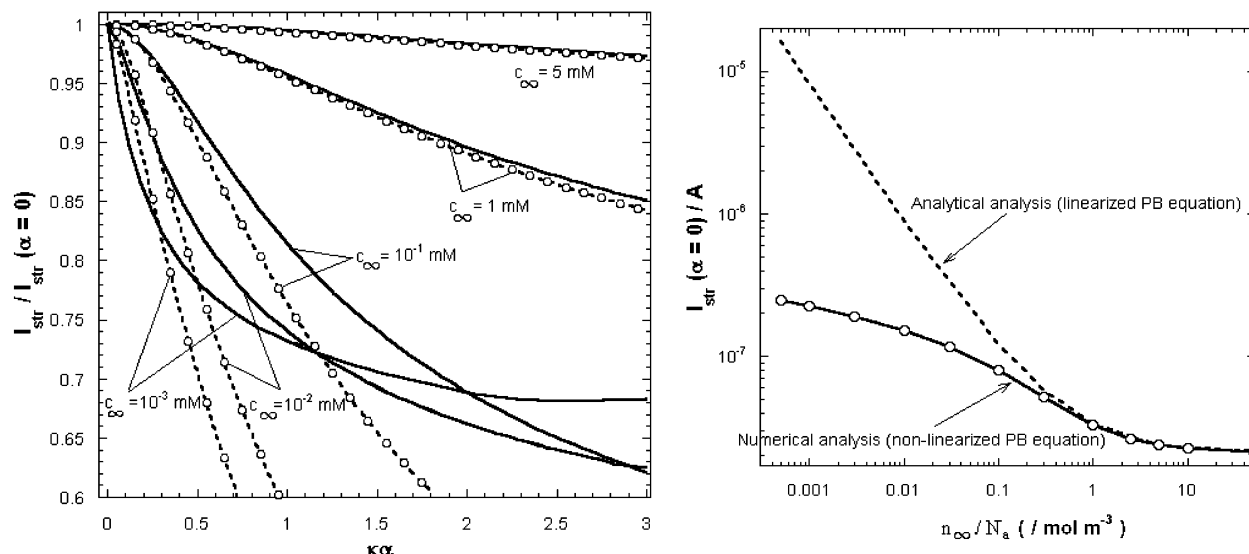
Figure 7. Representation of the streaming current I_{str}, normalized with respect to $I_{str}(\alpha = 0)$ (inset), as a function of $\kappa\alpha$ and c_∞ (indicated): plain lines, numerical results; points + dashed curves, results based on the analytical theory reported in ref 1. For comparison purposes, $I_{str}(a = 0)$ is given in the inset. Model parameters: $a = 0.2$ mm, $h/a = 0.1$, $\rho_o = 1$ mM, $\lambda_o^{-1} = 10$ nm.

5. Electrokinetics

5.1. Streaming Current. The streaming current, I_{str}, represents the charge transport due to flow. It is simply defined by the integral

$$I_{str} = 2l \int_0^{a/2+h} \rho_{el}(x)v(x)\,dx \qquad (66)$$
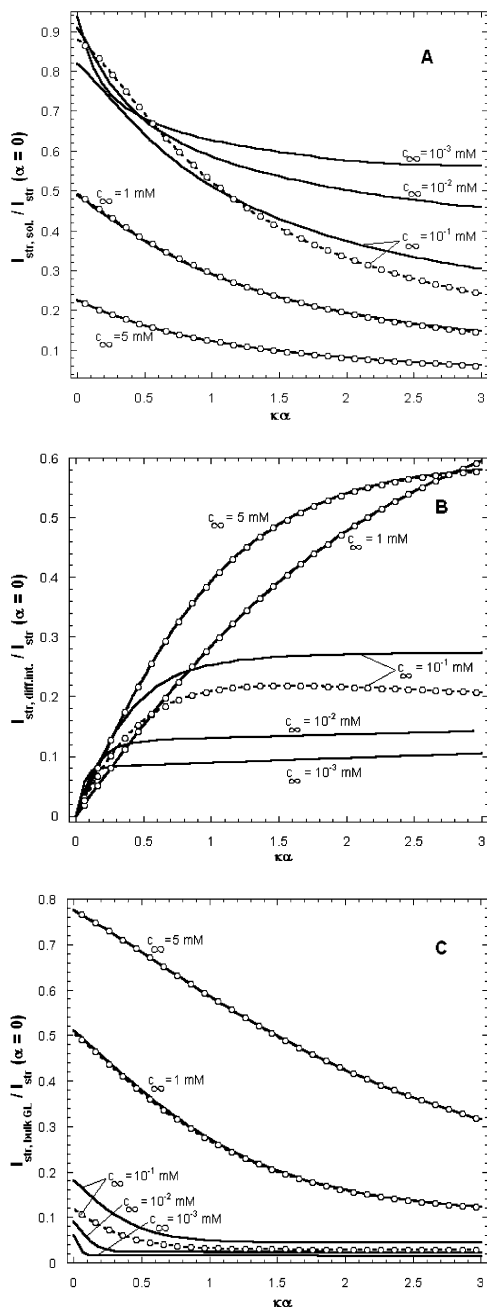
Following the notation adopted in ref 1, I_{str} can be split into its three constituents

$$I_{str} = 2l\left(\int_0^{a/2-\alpha} \rho_{el}(x)v(x)\,dx + \int_{a/2-\alpha}^{a/2+\alpha} \rho_{el}(x)v(x)\,dx + \int_{a/2+\alpha}^{a/2+h} \rho_{el}(x)v(x)\,dx\right) \quad (67)$$

where from left to right the integrals refer to the currents streaming in the solution, in the diffuse interface, and in the bulk gel layer, denoted as $I_{str,sol}$, $I_{str,diff\ int}$, and $I_{str,bulk\ GL}$, respectively. Each component can be evaluated either analytically (domain 1) or numerically (domains 2 and 3) from the potential and hydrodynamic velocity profiles as determined in sections 2 and 3, respectively. In Figure 7, we give typical results obtained for I_{str} as a function of the electrolyte concentration and thickness of the diffuse soft layer, i.e., $\kappa\alpha$. The results are normalized with respect to the quantity $I_{str}(\alpha = 0)$, which corresponds to the streaming current according to the step-function model of the interface (see inset Figure 7) and further compared with the predictions based on the Debye−Hückel approximation.[1] At very high electrolyte concentrations ($c_\infty > 5$ mM in the example given), the impact of $\kappa\alpha$ on the electrokinetics is limited if not absent since in that concentration range there are very few electrokinetically active countercharges inside and outside the diffuse interface (low Donnan potential). The interface then effectively corresponds to a sharp interface with a clear location for the plane separating the bulk gel layer and the electrolyte side. The numerical results are further very well fitted by the linear analysis in ref 1. When c_∞ is decreased, the presence of a spatial gradient for the interfacial electrostatics and hydrodynamics considerably affects the electrokinetic response. More exactly, an increase of the thickness α results in a decrease of the streaming current I_{str}. This major point was already encountered within the linear treatment of t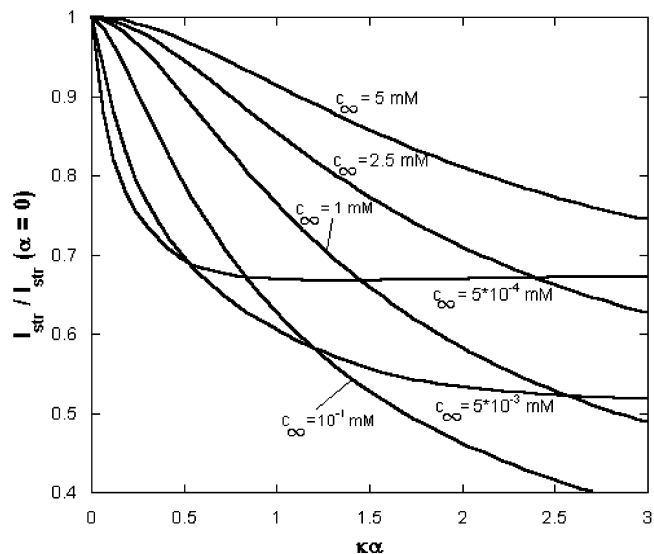he electrokinetics of diffuse soft layers.[1] Increase of α leads to a decrease of the hydrodynamic velocities $v(x)$ for the entire range of x (Figure 4) and to an increase of the local electric potentials, or equivalently of the local concentrations for the countercharges in the region $x < a/2$ (Figure 3A). The hydrodynamic effect overrules the electrostatic effect in the sense that a significant amount of potentially electrokinetically active ions are immobilized, thus leading to strong reduction of I_{str}. Upon further decrease of c_∞, new features appear. Whereas the analysis based on the linearization of the electrokinetic equations points at a systematic decrease of I_{str} in the complete $\kappa\alpha$ range, the rigorous numerical treatment reveals that for very low c_∞, I_{str} starts to develop a bend and may even slightly increase for values of $\kappa\alpha$ larger than unity. For these ranges of $\kappa\alpha$ and c_∞, the potential profiles are very asymmetric (Figure 3A), the potentials drastically increase in the region $x < a/2$. Hence the counterion concentration is significantly enhanced in the diffuse soft layer and the electrostatics dominates in the electrokinetics to such an extent that the ongoing decrease of the hydrodynamic velocity is outweighed. Since the asymmetry of the potential profiles cannot be predicted within the framework of the Debye−Hückel approximation (see ref 1), the behavior at low c_∞, and high $\kappa\alpha$ within that approximation is not only quantitatively but also qualitatively incorrect. Let us now have a closer look at the respective electrolyte concentration/$\kappa\alpha$-dependencies of the three contributions $I_{str,sol}$, $I_{str,diff\ int}$, and $I_{str,bulk\ GL}$ to the total current I_{str} (Figure 8). When increasing $\kappa\alpha$ at constant c_∞, $I_{str,bulk\ GL}$ (panel C) decreases because of the ensuing decrease of the fluid flow velocities (hydrodynamic effect) whereas the ratio $I_{str,bulk\ GL}/I_{str}$ ($\alpha = 0$) decreases while lowering c_∞ for a given $\kappa\alpha$. This is so because the increase of $I_{str}(\alpha = 0)$ upon decrease of c_∞ (inset Figure 7) is stronger than that of $I_{str,bulk\ GL}$ as resulting from the additional mobile charges in the region $x > a/2 + \alpha$ (see Figure 2C). For sufficiently low c_∞ and large $\kappa\alpha$, the electric potential equals the Donnan potential everywhere in domain 3 and the velocity there approaches the finite but nonzero value $\Delta P/\eta_w L_o\lambda_o^2$, so that the current $I_{str,bulk\ GL}$ is given by the limit

$$I_{str,bulk\ GL}\big|_{c_\infty \ll 1, \kappa\alpha \gg 1} = 2l(h - \alpha)\frac{\Delta P\rho_o}{\eta_w L_o\lambda_o^2} \qquad (68)$$

Figure 9. The same as in Figure 7, but for $\lambda_o^{-1} = 3.1$ nm. Only the numerical results are shown.

Figure 9 depicts curves such as those in Figure 7 for a larger bulk friction coefficient k_o. Qualitatively, the same comments may be given. Quantitatively, the current flowing in the bulk gel layer is strongly reduced so that the impact of $\kappa\alpha$ on the electrokinetic signal becomes more substantial (see the scales). An analysis of the components $I_{str,sol}$, $I_{str,diff\ int}$, and $I_{str,bulk\ GL}$ as a function of $\kappa\alpha$ and the flow penetration length λ_o^{-1} within the bulk gel layer would confirm that. The results are not shown but, basically, the trends correspond to those given in ref 1 for a gel layer with low Donnan potential. The reason is that variation of λ_o^{-1} modifies the hydrodynamic velocity profile, which, unlike the electroosmotic velocity distribution, does not depend on the actual shape of the potential distribution and y^D. The reader is referred to ref 1 for supplementary information.

5.2. Ohmic and Convective Components to the Total Back-Conduction Current, Streaming Potential. In the stationary state, the streaming current I_{str} equals the back-conduction current, denoted I_b, which consists of a bulk conduction contribution, denoted I_{mig}, resulting from the migration of the (mobile) ions under the action of the electric field E, and a convective component, I_{eo}, produced by the electroosmotic flow resulting from the action of the field on the diffuse double layer. I_{mig} and I_{eo} are given by the expressions
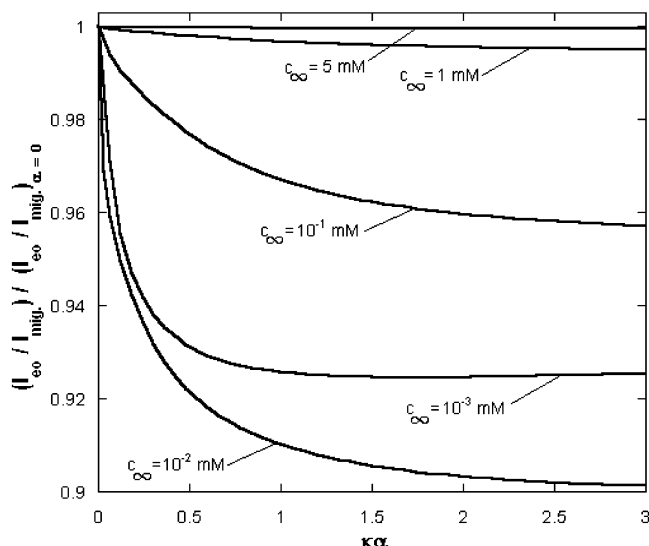
$$I_{mig} = 2lEc_\infty \int_0^{a/2+h} \{\lambda_- \exp[y(x)] + \lambda_+ \exp[-y(x)]\}\ dx \tag{69}$$

and

$$I_{eo} = 2l \int_0^{a/2+h} \rho_{el}(x)v_{eo}(x)\ dx \tag{70}$$

In eq 69, $\lambda_\pm$ represents the molar conductivities of the cations and anions from the 1:1 electrolyte. It is assumed that $\lambda_\pm$ are independent of the position x and equal the bulk aqueous solution values. This is justified for soft layers with high water content, as considered within this study. The integrals (69) and (70) were evaluated numerically from the potential and electroosmotic velocity profiles obtained in sections 2 and 4, respectively. For gel layers complying with $h \gg \alpha$ (as commonly met in practice[14]), the current I_{mig} remains practically independent of α. Figure 10 underlines the effect of α and c_∞ on

Figure 8. Respective contributions of (panel A) $I_{str,sol}$, (panel B) $I_{str,diff\ int}$, and (panel C) $I_{str,bulk\ GL}$ to the total current I_{str} streaming in the thin-layer chamber (which includes the charged layers): plain lines, numerical results; points + dashed curves (at the three largest electrolyte concentrations given), results based on the analytical theory reported in ref 1. Same parameters as in Figure 7.

Due to the aforementioned hydrodynamic and electrostatic effects, $I_{str,sol}$ (panel A) decreases and $I_{str,diff\ int}$ (panel B) increases with increasing $\kappa\alpha$. The positioning of the curves as computed for different electrolyte concentrations is according to expectation. Namely, the ratios $I_{str,sol}/I_{str}$ ($\alpha = 0$) increase and $I_{str,diff\ int}/I_{str}$ ($\alpha = 0$) decreases upon decrease of c_∞ at constant $\kappa\alpha$. This results from the enhancement for the concentration of mobile ions in domain 1/2 as compared to the overall amount of countercharges which determines $I_{str}(\alpha = 0)$. In passing, we note that the influence of the thickness of the diffuse interface on the currents plotted in Figures 7 and 8 is more pronounced at low $\kappa\alpha$ and low c_∞, the slopes $dI/d(\kappa\alpha)$ being the steepest in these regimes.

Figure 10. Effect of the thickness of the diffuse interface and electrolyte concentration (indicated) on I_{eo} (section 5.2 in the text). $a = 0.2$ mm, $h/a = 0.01$, $\rho_o = 1$ mM, and $\lambda_o^{-1} = 4.5$ nm. The parameters $\lambda_\pm$ required for the computation of I_{mig} refer to the ions Na^+ and Cl^-.

the current I_{eo}, plotted in the dimensionless form $(I_{eo}/I_{mig})/(I_{eo}/I_{mig})_{\alpha=0} \approx I_{eo}/(I_{eo})_{\alpha=0}$. The coupling between electrostatic and hydrodynamic profiles $y(x)$ and $v_{eo}(x)$ results in dependencies on α and c_∞ similar to those for I_{str} already explained (Figure 7). Besides, upon decrease of c_∞ (or h) at constant α (that is when lowering κh), the ratio I_{eo}/I_{mig} rapidly increases (but still remains much lower than 1 for practical values of h and λ_o), as expected (not shown). The lower the friction exerted by the polymer segments on the flow in the diffuse soft layer, the more significant is that increase (and the less apparent is the impact of $\kappa\alpha$). Description of the electrokinetics of thin soft layers corresponding to $\kappa h \approx 1$ or even lower requires consideration of the rigid surface, located at $x = a/2 + h$, for determining the potential distribution. If indeed this surface is charged, the counterion distribution across the diffuse interface is mediated not only by the distribution of fixed charges in the soft layer but also by the surface chemistry of the boundary on which it is grafted. The distribution of the friction coefficient in the vicinity of that boundary may also come into play when $\lambda_o h \approx 1$. These cases are more exotic than of practical use for the investigation of macroscopic three-dimensional gel layers, the difficulty then being to separate the electrokinetic contribution of the soft layer (which is the interesting one) from that of the boundary surface. This problem however becomes crucial when dealing with the electrophoresis of small charged colloidal particles (radius comparable with κ^{-1}) covered with (charged) thin polyelectrolyte film (of nanometer scale). It will be addressed in later communications on the electrophoresis of *diffuse soft particles*.

From the relation $I_{str} = I_b$ which holds at steady state, one derives the following expression for the streaming potential $\Delta\varphi_{str}$[1]

$$\Delta\varphi_{str} = \frac{I_{str}L_o}{\zeta(K_{mig} + K_{eo})} \quad (71)$$

where ζ is the cross section $(a + 2h)l$ of the cell, K_{mig} $(=I_{mig}/\zeta E)$ and K_{eo} $(=I_{eo}/\zeta E)$ representing the conductivity terms originating from the conductive and electroosmotic components of the total back-current. For $\kappa h \gg 1$ and $\kappa\lambda_o^{-1} \approx 1$, pertaining to the most common gel layers, we have $I_{eo}/I_{mig} \ll 1$ (discussed before) so that the patterns of $\Delta\varphi_{str}$ as a function of α and c_∞ are essentially those of I_{str}.

6. Conclusions

In this paper the concept of diffuse soft interfaces as introduced in ref 1 is applied to the electrokinetics of charged gels layers characterized by high Donnan potentials. For that purpose, the electrostatics, hydrodynamics, and electroosmosis are tackled on the basis of coupled seminumerical analyses of the nonlinearized Poisson−Boltzmann and Navier−Stokes equations, taking into account spatial distributions for the friction coefficient and fixed charge density across the diffuse interface. The electrokinetic properties of the diffuse soft layer are described and interpreted in terms of the electrostatic and hydrodynamic consequences of the finite thickness of the diffuse region on the potential and velocity profiles. Excellent agreement between linear analysis, as performed in ref 1, and nonlinear treatment of the electrokinetic equations is obtained for low values of the Donnan potential or equivalently relatively large electrolyte concentrations. Special attention is devoted to the electrokinetic behavior in the low electrolyte concentration regime, where the discontinuous approach by Ohshima largely overestimates the results obtained on the basis of a gradual transition for the electrostatic and hydrodynamic properties of the soft layer. The trends predicted by the theory proposed are in line with experimental data, which further clarify limitations of the Ohshima approach for strongly swollen soft layers.[14,15] In the third and last part of this series of papers,[14] streaming potential data collected for crossed-linked polyacrylamide gels with various charge densities in the range 0.5−0.05 mM electrolyte concentration will be quantitatively analyzed and successfully interpreted within the theoretical formalism developed in parts 1[1] and 2 (this study). In future communications, the theory for electrophoresis of soft particles[2] by Ohshima will be revisited and improved by treating the hydrodynamic and electrostatic properties of the polymer films on the basis of a continuum modeling.[19]

(19) Duval, J. F. L.; Ohshima, H. The Electrophoresis of Diffuse Soft Particles, submitted to *J. Phys. Chem. B*.